**HEFAT2010**
**7th International Conference on Heat Transfer, Fluid Mechanics and Thermodynamics**
**19-21 July 2010**
**Antalya, Turkey**

# EXPERIMENTAL STUDY OF FORCED CONVECTION HEAT TRANSFER AROUND TRIANGULAR CYLINDER IN CROSS FLOW

Ali M*, Zeitoun O. and Nuhait A.
*corresponding author
Department of Mechanical Engineering,
King Saud University,
P. O. Box 800, Riyadh, 11421,
Saudi Arabia,
E-mail: mali@ksu.edu.sa

## ABSTRACT

Experimental investigations have been reported on steady state forced convection from the outer surface of horizontal triangular surface ducts in cross flow of air. The triangular cylinder was set such that its vertex faces the flow. Four equilateral triangular ducts have been used with cross section side length of 0.03, 0.05, 0.08 and 0.12 m, corresponding to blockage ratios 0.066, 0.110, 0.175 and 0.263 respectively. The ducts are heated using internal constant heat flux heating elements. The temperatures along the surface and peripheral directions of the duct wall are measured. Local Nusselt numbers at the middle of the duct are obtained around the perimeter for the larger ducts 0.12 and 0.08 m for various Reynolds numbers. Total overall averaged Nusselt numbers are obtained for transition to turbulent regime and critical points are tabulated for turbulent distinction. Empirical correlations are obtained for the overall averaged Nusselt numbers and Reynolds number using the equilateral side length as a characteristic length. Furthermore, other general correlations are obtained for the overall averaged Nusselt number using the duct length as a characteristic length and the blockage ratio as a parameter.

## INTRODUCTION

Triangular cylinders in cross flow have many engineering applications in cooling of electronic components and heat exchangers. Survey of the literature shows that, correlations for the overall averaged Nusselt numbers for forced convection heat transfer from circular and non-circular cylinders have reported by different authors. Churchill and Bernstein [1] have reported a single comprehensive equation that cover the entire range of Reynolds number for circular cylinder in cross flow for a wide range of Prandtl number as follows:

$$\overline{Nu}_D = 0.3 + \frac{0.62 Re_D^{0.5} Pr^{1/3}}{\left[1+(0.4/Pr)^{2/3}\right]^{1/4}} \left[1+\left(\frac{Re_D}{282000}\right)^{5/8}\right]^{4/5} \quad (1)$$

Tables are also given for the empirical correlation to be used for noncircular cylinders in cross flow of gas by Eckert [2], Jakob [3], Gephardt [4] and Incropera and DeWitt [5]. Comprehensive archival correlations for average heat transfer coefficients for non-circular and circular cylinders and spheres in cross flow have reported by Sparrow et al. [6]. Numerical simulation of two dimensional flow over a circular cylinder using the immersed boundary method has reported by Silva et al [7]. An integral approach of the boundary layer analysis has employed to investigate fluid flow and heat transfer from an infinite circular cylinder in cross flow by Khan et al. [8]. Abbassi et al [9] have investigated the structure of laminar flow and heat transfer from a built-in triangular prism placed in a differentially heated channel. They obtained the critical Reynolds number, where the transition from symmetric to periodic flow, occurs at 45 with a blockage ratio of 0.25. Recently, numerical simulation of unconfined flow past a triangular cylinder is reported when the vertex of the triangle facing the flow for low Reynolds number by De and Dalal [10]. They obtain a critical Reynolds number of 39.9. Furthermore, De and Dalal [11] have extended their previous study for forced convection from a triangular cylinder placed in a channel for low Reynolds number and specific blockage ratio. The famous circular cylinder in cross flow to air and liquids has investigated by Sanitjai and Goldstein [12]. Other shapes in cross flow such as square, diamond, elliptical, hexagonal, and rectangular cylinder have investigated by Sharma and Eswaran [13], Yoo et al [14], Ota et al. [15], Hilpert [16] and Igarashi [17] respectively. The following correlations for square and diamond in cross flow have been cited by [17] and also recommended by [6] and are shown here for comparison respectively:

$$\overline{Nu}_L = 0.14 Re_L^{0.66}, \quad 5000 \le Re_L \le 60{,}000 \quad (2)$$

$$\overline{Nu}_L = 0.27 Re_L^{0.59}, \quad 6000 \le Re_L \le 60{,}000 \quad (3)$$

It should be noted that, L in Eq. (2) is the side of the square or the diamond cylinders. In all the cited papers the heat transfer

from triangular cylinders in unconfined cross flow have been studied only for the flow fields at small Re ≤ 200 and there is no correlation available in the literature to report the average heat transfer coefficient from such cylinders which motivates the current study.

The present investigation presents experimental study of heated triangular cylinders in cross flow of air. Local Nusselt numbers are obtained around the perimeter of the cylinders for vertex facing the flow. General correlations are obtained as function of Reynolds numbers and also as a function of the blockage ratio when the length of the duct is used as a characteristic length. The experiments have done for a large Reynolds numbers using four ducts.

## NOMENCLATURE

| | | |
|---|---|---|
| $A_s$ | [$m^2$] | duct total surface area, 3L H |
| $A_B$ | [$m^2$] | end plate cross section area |
| EIP | [W] | Electrical input power |
| h | [$Wm^{-2}K^{-1}$] | heat transfer coefficient |
| H | [m] | duct length |
| k | [$Wm^{-1}K^{-1}$] | thermal conductivity |
| L | [m] | equilateral triangle cross section side length |
| *l* | [m] | square side of the wind tunnel's test section |
| l | [m] | perimeter of the triangular cylinder |
| Nu | $\frac{\bar{h}L}{k}$, $\frac{\bar{h}H}{k}$, or $h_m L/k$ | average Nusselt number |
| $q_c$ | [$W/m^2$] | convection heat flux |
| $q_B$ | [$W/m^2$] | heat lost by conduction through the Bakelite end plates |
| $Re_L$ | [vL/v] | Reynolds number |
| T | [K] | Temperature |
| $T_{iB}$ | [K] | inside surface temperature of the Bakelite end plate |
| $T_{oB}$ | [K] | outside surface temperature of the Bakelite end plate |
| x | [m] | axial or longitudinal distance |

Special characters

| | | |
|---|---|---|
| $\mathcal{B}$ | [L/*l*] | blockage ratio |
| $\delta$ | [m] | Bakelite thickness |
| θ | [K] | arithmetic mean temperature defined by Eq. (8) |
| ν | [$m^2S^{-1}$] | kinematics viscosity |

Subscripts

| | |
|---|---|
| B | Bakelite |
| H | characteristic length |
| x | indices at the perimeter direction ranging from 1 to 3 at any station x. |
| L | characteristic length |
| m | indices at the perimeter direction ranging from 1 to 9 at the middle of the duct. |
| x | indices in the axial direction ranging from 1 to 5 |
| ∞ | ambient condition. |

## EXPERIMENT SET-UP AND PROCEDURE

Figure 1 shows a layout diagram of the variable, low-speed, blown type wind tunnel used in this experiment. The entrance section consists of a bell-mouth inlet duct (1), diffuser (2), settling length (3), contracting section (4) and the flow straightener sections (5, 6) followed by the test section (7) where the test triangular duct is placed. The test section is 1.26 m with a square cross-section of *l* = 0.456 m made from Plexiglas. The test triangular cylinder is held horizontally, normal to the air flow, 2.73 m from the entrance of the flow straightener section (5, 6) as seen in Fig. 1. The flow velocity is adjusted using flow control holes around the bell-mouth inlet duct of the fan. A pitot tube (8) is held in a vertical position, 1.22 m from the entrance of the flow straightener section and 1.51 m ahead of the test triangular cylinder. The maximum and

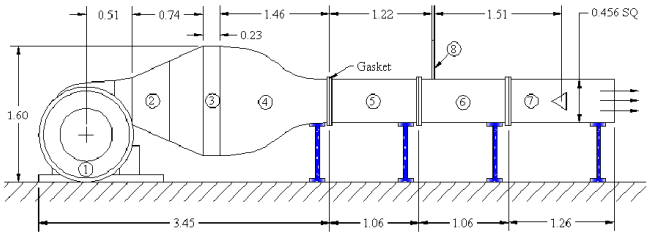


**Figure 1** Layout of the wind tunnel used in the experiment showing the location of the triangular cylinder, see text for details (all unit distances are in m).

minimum velocities measured by the pitot tube at the centerline of the straightener section are 17.25 m/s and 10.05 m/s respectively during this experiment. The velocity distribution in the vertical direction is shown in Fig. 2 for the maximum and minimum blower speeds. In this figure the velocity profiles are normalized by the maximum speed at the centerline corresponding to the maximum or minimum blower speeds and the vertical distance is normalized by the total vertical height *l* = 0.456 m of the straightener section. This figure also shows

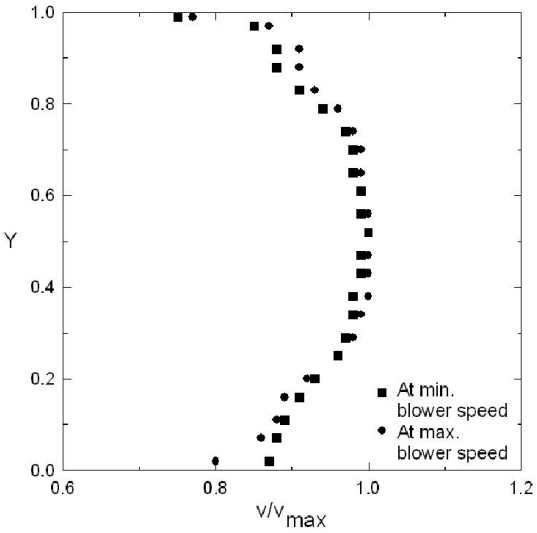


**Figure 2** Distribution of the stream velocity in the vertical direction of the wind tunnel at1.51 m ahead of the test triangular cylinder.

that the velocity is almost uniform around the centerline of the test section in the range where 0.2 < Y < 0.8. It should be noted that the test triangular duct is held horizontally at Y = 0.5 in the test section. The test triangular ducts are positioned such that the vertex of the triangle faces the flow. Four ducts are used with equilateral cross section side length of 0.03, 0.05, 0.08, and 0.12 m corresponding to blockage ratios β of 0.066, 0.110, 0.175, and 0.263 respectively, with duct length being 0.38 m. The ducts were made from brass of thickness 0.0015 m (D) (polished to reduce any possible radiation). An electrical

heating element (H) (0.0066 m O.D.) was inserted into the center of each duct as seen at Fig. 3. Bakelite end plates (B) (thermal conductivity = 0.15 W/mK [18]) 0.0206 m thick were attached at both ends of each test duct to reduce the rate of heat loss from the duct ends by conduction (Fig. 3).

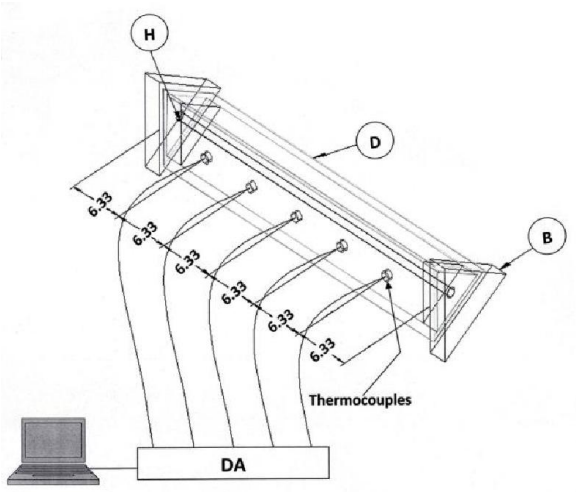


**Figure 3** The triangular cylinder (D) showing the axial thermocouple locations, Bakelite end plates (B), heating element (H), data acquisition system (DA) and the lab top used in the experiment. The perimeter thermocouples are not shown, see text for details.

The surface temperatures are obtained at five points 0.063 m apart in the longitudinal direction of each duct at the three equilateral surfaces as seen in Fig. 3. For the large triangular cylinders of sides L = 0.12 m and 0.08 m; two more thermocouples are evenly installed on the surface in the perimeter direction at the middle of each surface (not shown in Fig. 3). Twenty one calibrated Chromel- Alumel (type K) self adhesive thermocouples (0.3 seconds time response with flattened bead) were stuck on the duct surfaces for ducts having L = 0.12 m and 0.08 m whereas fifteen are used for the small ducts having L = 0.03 m and 0.05 m. Two more thermocouples were stuck on the outer surface of the Bakelite end plates; one at each plate. To measure the heat lost by conduction, two thermocouples ( $0.01''$ or 0.25 mm diameter; one at each plate) were inserted through the Bakelite thickness and leveled with its inside surface. The ambient air temperature was measured by one more thermocouple supplied with the pitot tube (8) at the center line of the air flow.

The duct was oriented horizontally such that the vertex of the triangle facing the flow. Those thermocouples were connected to thirty channels data acquisition system (DA), which in turn were connected to a computer where the measured temperatures were stored for further analysis as seen in Fig. 3.

The input electrical power to the heating element (H); is controlled by a voltage regulator. The power consumed by the duct is measured by a Wattmeter and assumed uniformly distributed along the duct length. The heat flux per unit surface area of the duct is calculated by dividing the consumed power (after deducting the heat loss by axial conduction through the Bakelite end plates) over the duct outer surface area.

The maximum input power to the duct was chosen and set such that the maximum surface temperature does not exceed 160°C (thermocouples limit). Then the blower is turned on at the lower speed for almost one hour where the surface temperatures reach steady state. At this specific speed, a digital manometer is used to measure the dynamic pressure and the surface temperatures are also stored for further analyses. This process is repeated between eight or fifteen times for each duct at different speeds of the blower up to the maximum speed of the blower keeping the input power as a constant. The procedure outlined above is used to generate forced convection heat transfer data for triangular cylinders in cross flow of air for different Reynolds number range of 18631.00 to 128630.60.

## ANALYSES OF THE EXPERIMENT

The heat lost by radiation from the duct surface is estimated at the larger duct to be 1.58 % at most of the heat supplied. Therefore, the effect of radiation is neglected in the calculations and the heat generated inside the duct wall is assumed to be dissipated from the duct surface by forced convection and by axial conduction through the Bakelite end plates.

$$\text{EIP} = \text{Electrical input power} = A_s\, q_c + A_B\, q_B \qquad (4)$$

Where $A_s$ is the duct total surface area, $A_B$ is the Bakelite surface area normal to the heat transfer by conduction through the end plates and $q_c$ is the fraction of the heat flux dissipates from the duct surface by forced convection. The heat flux lost by axial conduction through the Bakelite end plates ( $q_B$ ) can be calculated as:

$$q_B = k_B \frac{(T_{iB} - T_{oB})}{\delta} \qquad (5)$$

Measurements show that, the fraction of the axial conduction heat lost through the Bakelite end plates is 1.8 % at most of the total input power. In Eq. (5); $T_{iB}$ and $T_{oB}$ are the measured inside and outside surface temperatures of the Bakelite end plates, respectively and $k_B$ and $\delta$ present the Bakelite thermal conductivity and thickness, respectively.

### *Local heat transfer coefficient*

In this case the local heat transfer coefficient is estimated around the perimeter of the triangular cylinder (L = 0.12 and 0.08 m) at the middle, where there are three thermocouples at each side surface to catch the local changes of the heat transfer coefficient which can be estimated as:

$$h_m = \frac{q_c}{T_m - T_\infty}, \quad m = 1,2,\ldots,9 \qquad (6)$$

And the corresponding local Nusselt number is:

$$(Nu_L)_m = \frac{h_m L}{k}, \quad m = 1, 2,\ldots,9 \qquad (7)$$

All physical properties are evaluated for each Reynolds number at constant $q_c$ at the local mean temperature $\theta_m$ as:

$$\theta_m = 0.5(T_m + T_\infty), \quad m = 1,2,\ldots..,9 \qquad (8)$$

### *Total overall averaged heat transfer coefficient*

In this case the perimeter averaged surface temperature at any station x in the longitudinal direction for each Reynolds number (run) is determined as:

$$T_x = \sum_{j=1}^{3} T_{xj} / 3, \quad (9)$$

where j presents the thermocouples in the perimeter direction at any station x along the surface of the duct. The arithmetic mean surface temperature is calculated along the axial direction for each run as:

$$\theta_x = 0.5(T_x + T_\infty), \quad x = 1,2,\ldots..,5 \quad (10)$$

Therefore for each Reynolds number there are five $T_x$ longitudinal temperature measurements. Consequently, once the electrical input power to the duct is measured, $q_B$ from Eq. (5) and $q_c$ from Eq. (4) then the axial (perimeter averaged) heat transfer coefficient $h_x$ can be calculated from:

$$h_x = \frac{q_c}{T_x - T_\infty}, \quad x = 1,2,3,\ldots,5 \quad (11)$$

and then the overall average $\bar{h}$ is obtained as:

$$\bar{h} = \sum_{x=1}^{5} h_x / 5 \quad (12)$$

Therefore, at each Reynolds number $Re_L$ there is only one overall averaged heat transfer coefficient. All perimeter averaged physical properties are first obtained at $\theta_x$ then the overall averaged properties are obtained the same way following Eq. (12). The non-dimensional overall averaged Nusselt number is defined using either the duct length as a characteristic length H = 0.38 m or one side of the equilateral cross section triangle L as a characteristic length as:

$$\overline{Nu}_H = \frac{\bar{h} H}{k}, \quad \text{or} \quad \overline{Nu}_L = \frac{\bar{h} L}{k} \quad (13)$$

In both cases the non-dimensional Reynolds number using the triangular side length as a characteristic length is used:

$$Re_L = \frac{v L}{\nu} \quad (14)$$

***Experimental uncertainty***

In this section, the experimental uncertainty is to be estimated in the calculated results on the basis of the uncertainties in the primary measurements. The error in measuring the temperature and in calculating the surface area is ± 0.2 $^oC$ and ± 0.003 $m^2$, respectively. The accuracy in measuring the voltage is taken from the manual of the Wattmeter as 0.5 % of reading ± 2 counts with a resolution of 0.1 V and the corresponding one for the current is 0.7 % of reading ± 5 counts + 1 mA with a resolution of 1 mA. The error in measuring the dynamic pressure is ± 0.1 Pa. At each run, forty scans of the temperature and the dynamic pressure measurements are made by the digital manometer and the data acquisition system, respectively for each channel and the mathematical average of these scans is obtained for both temperature and pressure. Therefore, using the above mentioned errors turns to maximum itemized uncertainties of the calculated results shown in Table 1 using the method recommended by Moffat [19].

**RESULTS AND DISCUSSIONS**

Experimental results for the variation of the local Nusselt number with the perimeter of the triangular cylinder (l) are shown in Figure 4 for the triangular cylinders in cross flow of air when the vertex faces the flow for the duct length L = 0.12 m for various Reynolds numbers. Solid circle symbols in the figure illustrate the thermocouple locations on the triangular sides. Solid lines connecting these points on one surface are followed by dashed lines up to the next surface's points following the path a, b, c and back to a as in Fig. 4. As expected, the results are strongly influenced by the nature of the boundary layer development on the surface. The $Nu_L$ variations show that, along the upper surface a b the profiles reach a minimum almost at the middle of the upper inclined surface at l/L = 0.5 and as $Re_L$ increases (> $10^5$) this minimum is moved a little further on the surface as illustrated in Fig. 4. At this minimum, the separation occurs and $Nu_L$ increases with l/L due to mixing associated with vortex formation in the wake up to

**Table 1** The maximum percentage uncertainties of various quantities for the triangular cylinder in cross flow.

| Quantity | Uncertainties (%) ◀or ▶ |
|---|---|
| *EIP* | 1.63 |
| $q_B$ | 12.67 |
| $q_c$ | 1.65 |
| $\bar{h}$ | 1.97 |
| $\overline{Nu}_L$ | 3.86 |
| $Re_L$ | 4.56 |

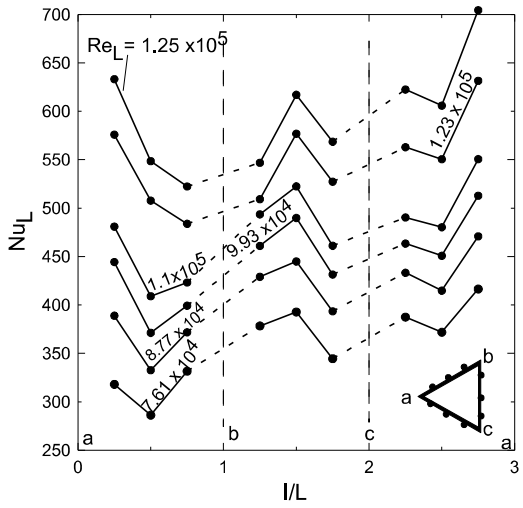


**Figure 4** Local Nusselt number distribution for air flow normal to a triangular cylinder for the duct has L = 0.12 m.

the second stagnation point at the middle of the rear surface b c at l/L = 1.5. It is also noticed that, the heat transfer coefficients lead to individual maximum at both the front stagnation point a and at the rear one at l/L = 1.5. Furthermore, the value of the coefficient on the rear face is larger than that on the front face similar to the diamond cylinders in cross flow [17]. Furthermore, following the path from the forward stagnation point a to the rear stagnation point across a b shows that it has one minimum, however the other path across a c has two minimums. It also should be noticed that, as $Re_L$ increases, $Nu_L$ increases sharply due to boundary layer transition to turbulent. Figure 5 shows similar variations for $Nu_L$ for the triangular cylinder L = 0.08 m for the vertex facing the flow. Figure 6

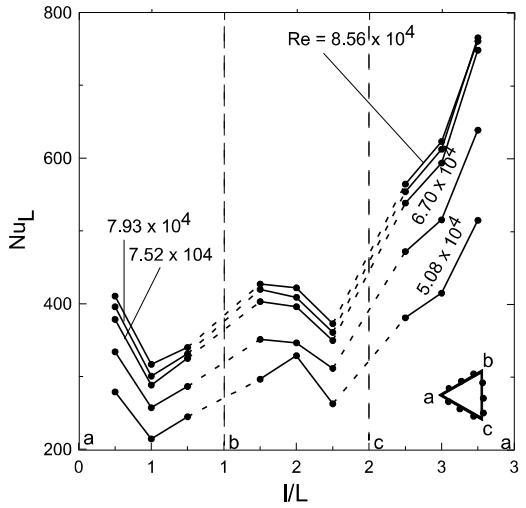


**Figure 5** Local Nusselt number distribution for air flow normal to a triangular cylinder for the duct has L = 0.08 m.

shows the overall variation of the average $\overline{Nu}_L$ verses the Reynolds number for the four triangular cylindrical ducts used for the case where the vertex facing the flow. This figure shows that $\overline{Nu}_L$ increase as $Re_L$ increase in the transition region, however with further development of the turbulent boundary layer, $Nu_L$ begins to decline as seen in the figure on the right of the dashed lines for ducts with L = 0.05, 0.08 and 0.12 m. The coordinates of the critical Nusselt numbers and Reynolds numbers where turbulent begins are shown in Table 2. However, from the standpoint of engineering calculations; empirical correlations are obtained for the overall average conditions as seen in Fig. 7. Solid line presents the correlation for the vertex of the triangular cylindrical ducts facing the flow as:

$$\overline{Nu}_L = 0.008 \quad (Re_L)^{0.95}, 1.8x10^4 \le Re_L \le 1.28x10^5 \qquad (15)$$

with a correlation coefficient R = 98.9 % and with error bands of ± 15 % where almost all of the data fall within these bands. Figure 8 shows the overall averaged Nusselt numbers using the uniform duct length H = 0.38 m as a characteristic length vs. the Reynolds numbers where the dada is correlated using the blockage ratio β = L/*l* as a parameter. It should be noted that, since the uniform length scale H is used then, a geometric

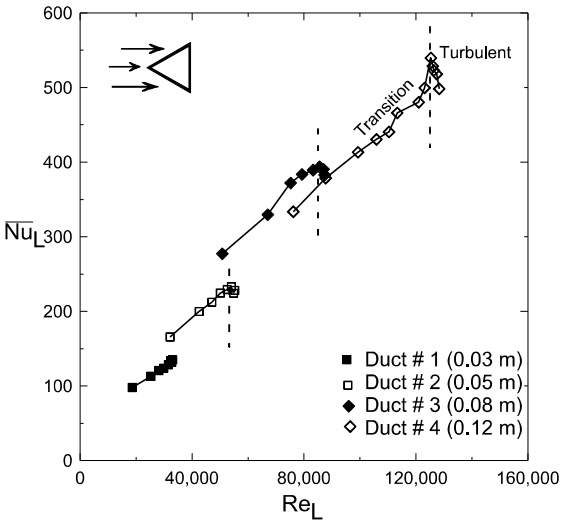


**Figure 6** The overall averaged Nusselt numbers for triangular cylinders in cross flow showing the transition and turbulent regimes.

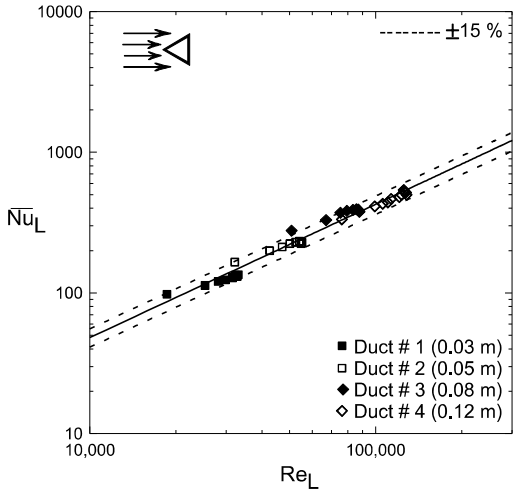


**Figure 7** The overall averaged Nusselt numbers for triangular cylinders in cross flowshowing the empirical correlation (solid line) for transition and turbulent regimes.

parameter (blockage ratio β) is necessary to characterize each duct as seen in Fig. 8. In this figure, the solid lines present the fitting correlation and the dashed lines present the maximum and minimum error bands of ± 15 % where all the data points fall within these bands. The correlation for the ducts have vertex facing the flow is given by:

$$Nu_H = 0.266\, Re_L^{0.667}\, \beta^{-0.686} \qquad (16)$$

Figure 9 is constructed to compare our results of isoflux surface with the close available correlations in the literatures such as Eq. (1) for circular cylinder in cross flow of air by [1] and Eq. (3) for diamond in cross flow of air reported by [17]. This comparison is shown in Fig. 9 for the overall Nusselt number Figure 9 is constructed to compare our results of isoflux surface

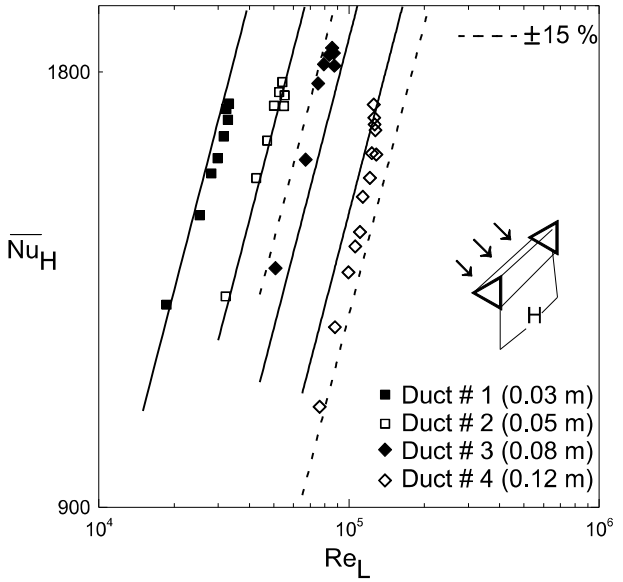


**Figure 8** The overall averaged Nusselt numbers for triangular cylinders in cross flow showing the empirical correlation (solid line) for transition regimes using β as a parameter.

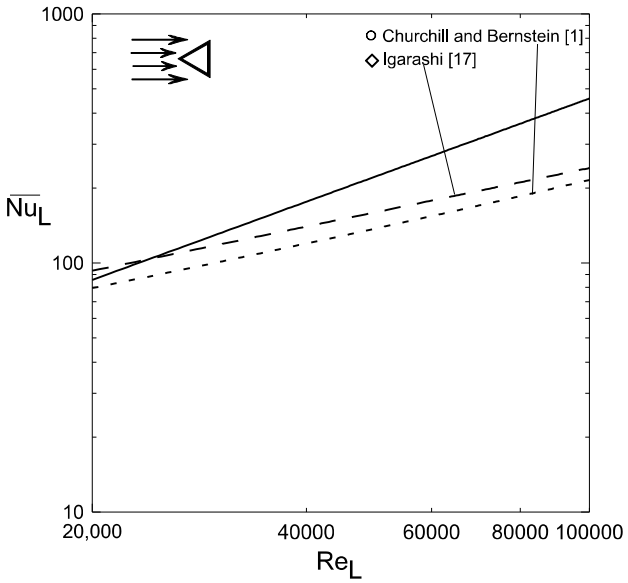


**Figure 9** Comparison of the overall averaged Nusselt numbers of the current results with [1] for circular cylinder in cross flow and with [17] for diamond cylinder in cross flow.

with the close available correlations in the literatures such as Eq. (1) for circular cylinder in cross flow of air by [1] and Eq. (3) for diamond in cross flow of air reported by [17]. This comparison is shown in Fig. 9 for the overall Nusselt number for vertex facing the flow presented by Eq. (15) as a solid line with the correlations for circular cylinder and diamond in cross flow given by Eqs. (1) and (3) respectively. It is clear that the current correlation has a future which captures a transition and turbulent of the flow in the rear part of the triangular cylinder at higher Reynolds number however, the other both equations are valid only up to $Re_L$ = 60,000. Therefore, as $Re_L$ increases the deviation in $Nu_L$ is expected to increase since the slope of the current correlation is higher than the other equations. It can be seen that using triangular cylinders in cross flow enhance the heat transfer over that of circular or diamond cylinders specially, at higher Reynolds number.

## CONCLUSIONS

Experimental study has been made on forced convection heat transfer from horizontal equilateral triangular cylinders in cross flow of air. Local Nusselt numbers around the perimeter of the ducts are observed to decrease at the beginning up to the separation points and then increase in the transition regime up to the turbulent limit where they decrease again. Critical points to separate the transition and turbulent regimes are obtained and tabulated for the larger ducts. Overall averaged Nusselt numbers are correlated with the Reynolds numbers for vertex facing the flow using the side length of the triangular cylinder ducts (Eqs. (15)). On the other hand, the overall averaged Nusselt numbers are correlated with Reynolds number as well as the blockage ratio when the length of the ducts is used as a characteristic length (Eqs. (16)). Comparison with circular and diamond cylinders in cross flow of air show that using triangular cylinder duct enhances the heat transfer at large Reynolds number.

**Acknowledgments**

This experimental investigation is supported by Saudi Arabian Basic Industrial Company (SABIC) and the Research Center, College of Engineering at King Saud University under the project No. 17/428. This support is highly appreciated and acknowledged.

Table 2. Critical values of the average Nusselt and Reynolds numbers where turbulent starts.

| | $Re_L$ | | $\overline{Nu}_L$ | | $\overline{Nu}_H$ | |
|---|---|---|---|---|---|---|
| L, m | ◄ | ► | ◄ | ► | ◄ | ► |
| 0.12 | 125295.70 | 108054.55 | 535.11 | 515.85 | 1694.53 | 1620.87 |
| 0.08 | 85571.30 | 81750.84 | 393.75 | 378.66 | 1870.30 | 1798.61 |
| 0.05 | 54051.20 | ------ | 233.13 | ------ | 1771.80 | ------ |

**References**


1- Churchill, S. W. and Bernstein M., "A correlating equation for forced convection from gases and liquids to a circular cylinder in cross flow", J. Heat Transfer Vol. 99, pp. 300-306, 1977.

2- Eckert, E. R. G., Introduction to the Transfer of Heat and Mass, McGraw-Hill, New York, 1950.

3- Jakob, M., Heat Transfer, vol. 1, John Wiley and Sons, Inc., New York, 1949.

4- Gebhardt, B., Heat Transfer, McGraw-Hill, New York, 1961.

5- Incropera, F. P., and DeWitt, D. P., "Introduction to Heat Transfer, fifth ed., John Wiley and Sons Inc., New York, 2002.

6- Sparrow, E. M., Abraham, J. P. and Tong, J. C. K., "Archival correlations for average heat transfer coefficients for non-circular and circular cylinders and for spheres in cross-flow", Int. J. of Heat and Mass Transfer, vol. 47, pp. 5285-5296, 2004.

7- Silva, A. L. F. L., Silveira-Neto, A. and Damasceno, J. J. R., "Numerical simulation of two-dimensional flows over a circular cylinder using the immersed boundary method", J. of Computational Physics, vol. 189, pp. 351- 370, 2003.

8- Khan, W. A., Culham, J. R. and Yovanovich, M. M., "Fluid flow around and heat transfer from an infinite circular cylinder", ASME, J. of Heat Transfer, vol. 127, pp. 785-790, 2005.

9- Abbassi, H., Turki, S. and Ben Nasrallah, S., "Numerical investigation of forced convection in a horizontal channel with a built-in triangular prism", ASME, vol. 124, No. 3, pp. 571- 573, 2002.

10- De, A. K. and Dalal, A., "Numerical study of laminar forced convection fluid flow and heat transfer from a triangular cylinder placed in a channel", ASME, J. of Heat Transfer vol. 129, pp. 646- 656, 2006.

11- De, A. K. and Dalal, A., "Numerical simulation of unconfined flow past a triangular cylinder", Int. J. for Numerical Methods in Fluids, vol. 52, pp. 801- 821, 2006

12- Sanitjai, S. and Goldstein, R. J., "Forced convection heat transfer from a circular cylinder in crossflow to air and liquids", Int. J. of Heat and Mass Transfer, vol. 47, pp. 4795- 4805, 2004.

13- Sharma, A. and Eswaran, V., "Heat and fluid flow across a square cylinder in the two-dimensional laminar flow regime", Numerical Heat Transfer, Part A- Applications, vol. 45, No. 3, pp. 247- 269, 2004.

14- Yoo, S. Y., Goldstein, R. J., and Chung, M. K., "Effects of angle of attack on mass transfer from a square cylinder and its base plate", Int. J. Heat Mass Transfer, vol. 36, pp. 371-381, 1993.

15- Ota, T., Aida, S., Tsuruta, T. and Kaga, M., "Forced convection heat transfer from an elliptic cylinder of axis ratio1: 2, Bull. JSME, vol. 26, pp. 262- 267, 1983.

16- Hilpert, R., "Warmeabgabe von heheizten drahten und rohrem im iuftsstrom", Forsch. Geb. Ingenieurwes, vol. 4, pp. 215- 224, 1933.

17- Igarashi, T., "Fluid flow and heat transfer around rectangular cylinders (the case of a width/height ratio of a section of o.33- 1.5)", Int. J. Heat Mass Transfer, vol. 30, pp. 893- 901, 1987.

18- William, D. and Callister, Jr., 2003, *Materials Science and Engineering An Introduction*, 6th ed, John Wiley & Sons, USA, Chap. 19. p. 660.

19- Moffat, R. J., 1988, "Describing Uncertainties in Experimental Results" Exp. Therm. Fluid Sci., **1** (1), pp. 3-7.